Available online at www.sciencedirect.com
ScienceDirect
Journal of Structural Biology xxx (2006) xxx–xxx
Journal of Structural Biology
www.elsevier.com/locate/yjsbi

# Spatial distribution and orientation of dermatan sulfate in human medial collateral ligament

Heath B. Henninger [a,b], Steve A. Maas [a,b], Clayton J. Underwood [a,b], Ross T. Whitaker [b], Jeffrey A. Weiss [a,b,c,*]

[a] Department of Bioengineering, University of Utah, 50 S Central Campus Drive, Rm. 2480, Salt Lake City, UT 84112, USA
[b] Scientific Computing and Imaging Institute, University of Utah, 50 S Central Campus Drive, Rm. 3490 Salt Lake City, UT 84112, USA
[c] Department of Orthopaedics, University of Utah, 30 North 1900 East, Rm. 3B165, Salt Lake City, UT 84132, USA

Received 26 April 2006; received in revised form 1 September 2006; accepted 5 October 2006

**Abstract**

The proteoglycan decorin and its associated glycosaminoglycan (GAG), dermatan sulfate (DS), regulate collagen fibril formation, control fibril diameter, and have been suggested to contribute to the mechanical stability and material properties of connective tissues. The spatial distribution and orientation of DS within the tissue are relevant to these mechanical roles, but measurements of length and orientation from 2D transmission electron microscopy (TEM) are prone to errors from projection. The objectives of this study were to construct a 3D geometric model of DS GAGs and collagen fibrils, and to use the model to interpret TEM measurements of the spatial orientation and length of DS GAGs in the medial collateral ligament of the human knee. DS was distinguished from other sulfated GAGs by treating tissue with chondroitinase B, an enzyme that selectively degrades DS. An image processing pipeline was developed to analyze the TEM micrographs. The 3D model of collagen and GAGs quantified the projection error in the 2D TEM measurements. Model predictions of 3D GAG orientation were highly sensitive to the assumed GAG length distribution, with the baseline input distribution of $69 \pm 23$ nm providing the best predictions of the angle measurements from TEM micrographs. The corresponding orientation distribution for DS GAGs was maximal at orientations orthogonal to the collagen fibrils, tapering to near zero with axial alignment. Sulfated GAGs that remained after chondroitinase B treatment were preferentially aligned along the collagen fibril. DS therefore appears more likely to bridge the interfibrillar gap than non-DS GAGs. In addition to providing quantitative data for DS GAG length and orientation in the human MCL, this study demonstrates how a 3D geometric model can be used to provide *a priori* information for interpretation of geometric measurements from 2D micrographs.


*Keywords:* Ligament; Decorin; Glycosaminoglycan; Dermatan sulfate; Geometric model

## 1. Introduction

Ligaments are collagen-based tissues that resist abnormal joint motions by connecting bone to bone. Ligament is approximately 70% Type I collagen by dry weight (Amiel et al., 1990), with the balance of the hydrated tissue consisting of "ground substance", which is a gel-like mixture of proteins, proteoglycans (PGs), glycosaminoglycans (GAGs), and water surrounding the ordered collagen fibrils. GAGs in ligament constitute 0.2–5.0% of the total dry weight (Amiel et al., 1984; Gillard et al., 1977). Although only a small percentage of tissue, understanding the distribution and structural organization of GAGs in ligament may shed light on the role of these important molecules.

Decorin, a small leucine-rich PG, has been demonstrated to play diverse roles in connective tissues, ranging from regulation of collagen fibril formation (Vogel et al., 1984) to affecting the mechanical properties of the tissue (Danielson et al., 1997; Robinson et al., 2005). Decorin is the most

* Corresponding author. Tel.: +1 801 587 7833; fax: +1 801 585 5361.
*E-mail address:* jeff.weiss@utah.edu (J.A. Weiss).

1047-8477/$ - see front matter © 2006 Published by Elsevier Inc.
doi:10.1016/j.jsb.2006.10.008

prevalent PG species in ligaments in terms of molar quantity (Ilic et al., 2005) and it localizes to (or "decorates") the surface of collagen fibrils in a repeating fashion (Pringle and Dodd, 1990). The decorin core protein is thought to be either a horseshoe- or banana-shaped molecule and to straddle a single collagen triple helix, binding every 67 nm along the fibril surface at the D-period band gap in the tropocollagen quarter-stagger pattern (Scott, 1996; Scott and Orford, 1981; Scott et al., 2004). The exact 3D conformation of decorin, including whether it functions as a monomer or dimer, remains a subject of debate (Goldoni et al., 2004; Scott, 2003; Scott et al., 2004; Weber et al., 1996). Depending on the tissue, either a single dermatan sulfate (DS) or a single chondroitin sulfate (CS) GAG side chain is covalently bound near the amino terminus of the decorin core protein (Chopra et al., 1985). This binding site allows a single DS chain to be exposed to the interfibrillar space. Conformational flexibility within the iduronate residues along the DS backbone may yield the flexibility to align the GAG in many possible orientations with respect to the collagen fibril (Scott, 1992; Venkataraman et al., 1994). DS chains can self-associate under physiological conditions, containing up to 10 or more individual GAG chains as an aggregate (Ernst et al., 1995; Scott, 1992). It should be noted that the biglycan PG, although significantly less prevalent than decorin in ligament (Ilic et al., 2005), contains two GAG side chains, either DS and/or CS (Trowbridge and Gallo, 2002).

The GAG side chain of decorin has been described as forming interfibrillar proteoglycan bridges by aggregation of GAG chains from adjacent collagen fibrils (Scott, 2001; Scott and Thomlinson, 1998) and the bridges have been suggested to play a direct role in the mechanical integrity of tendons (Liu et al., 2005; Redaelli et al., 2003; Vesentini et al., 2005). The interfibrillar bridges have been proposed to elastically sustain mechanical stresses in fibrous collagen-based tissues through a reversible longitudinal slippage model (Scott and Thomlinson, 1998). Within that model, GAG chains may act as a lubricant between adjacent collagen fibrils, cushioning compressive forces (Scott, 2003). Recent research has attempted to quantify mechanical interactions in the collagen–decorin–DS bond chain (Liu et al., 2005). Liu quantified the GAG–GAG association to be the weakest link, overcome by strong attractive forces between the decorin core protein and tropocollagen molecule, and weaker still than the decorin–DS bond at the protein–GAG interface, supporting the mechanism of the longitudinal slippage model.

Although DS GAGs have been qualitatively described as oriented roughly orthogonal to collagen fibrils in various tissues (Cribb and Scott, 1995; Kuwaba et al., 2001; Raspanti et al., 1997, 2002; Scott, 1988; Scott and Orford, 1981; Scott and Thomlinson, 1998; Van Kuppevelt et al., 1987), quantitative data for their spatial distribution and orientation in any connective tissue are unavailable. Further, although other species of large sulfated GAGs have been shown interspersed between and along the collagen fibrils (Raspanti et al., 1997, 2002; Van Kuppevelt et al., 1987), the relative proportions and species of sulfated GAGs at each orientation have yet to be determined. Understanding how GAGs are oriented and distributed with respect to collagen fibrils has implications ranging from tissue modeling to gaining a broader understanding of molecular-level material symmetries and mechanics.

To date, existing models of GAG mechanics within fibrous connective tissues have assumed perfectly orthogonal GAG symmetry with respect to neighboring collagen fibrils (Redaelli et al., 2003). Measurements of three-dimensional (3D) GAG orientation are complicated by the fact that the primary method of viewing has been with two-dimensional (2D) TEM micrographs. When GAG structure and orientation are examined in 2D TEM micrographs, information is lost. The viewer is unable to tell if a GAG is leaving the viewing plane or is contained wholly within the preparation, if a GAG overlaps another in the viewing plane, or the exact three-dimensional orientations with respect to the neighboring collagen fibrils.

The objectives of this study were to quantitatively determine the quantity, length, and 3D orientation of DS GAGs in the human medial collateral ligament (MCL). To achieve this goal, we created a 3D geometric model of sulfated GAGs interspersed within an array of collagen fibrils, and used this model to interpret measurements of apparent quantity, length, and orientation from 2D TEM images. Digestion with chondroitinase B (ChB, an enzyme that specifically degrades DS) was used to distinguish DS GAGs from non-DS GAGs. Custom image processing software was written to allow reliable segmentation of stained GAGs in 2D TEM images.

## 2. Methods

### 2.1. Collagen/GAG model inputs

A 3D geometric model of collagen and GAGs in tendon and ligament was created using parameters for collagen fibril diameter, fibril area (cross-section), GAG length, and GAG distribution. It should be noted that when DS GAGs are described in the models and 2D TEM images, these structures are likely aggregates of at least two GAGs. Collagen fibril diameter varies by tissue but not necessarily by species (Fung et al., 2003). Measurements of collagen fibril diameter from various tendons and ligaments place the range from 50 to 200 nm and measurements of the ratio of collagen cross-sectional area to total transverse cross-sectional area range from 40 to 70% (Baek et al., 1998; Frank et al., 1989; Fung et al., 2003; Hart et al., 1999; Lo et al., 2004; Silver et al., 2003). In the baseline model, collagen fibrils were assigned a diameter range of 90–110 nm and collagen area as a proportion of total transverse cross-sectional area was targeted at 50–65%.

A study of decorin PGs using rotary shadowing electron microscopy provides realistic measurements of their 3D length. Decorin PGs from bovine tendon were isolated onto a



Please cite this article in press as: Henninger, H.B. et al., Spatial distribution and orientation of dermatan sulfate in human medial collateral ligament, J. Struct. Biol. (2006), doi:10.1016/j.jsb.2006.10.008

fixed plane before imaging (Morgelin et al., 1989). Small single GAG chain PGs, likely decorin, assumed a near-Gaussian length distribution with a mean of 69 ± 23 nm. The core protein appeared to be only a small fraction of the overall length. This profile of GAG lengths was used in the baseline geometric model to represent the DS population in ligament.

The spatial distribution of GAGs in the model was quasi-random with respect to the collagen fibrils. GAG angle was not constrained, rather GAGs were allowed to project from collagen fibrils at any angle so long as they did not occupy the space taken up by another GAG or a collagen fibril.

### 2.2. Collagen/GAG model generation

Given the parameters stated previously, a highly controllable and repeatable 3D computer model of a 3D collagen/GAG matrix was programmed using C++. Collagen was generated in a quasi-hexagonal packing scheme, using a "jitter" parameter to introduce deviations from perfect crystalline organization. A seed (random number) created a unique collagen pattern and therefore a unique GAG distribution. Any given model could be repeated by using the same seed. An executable version of the software, which runs under the Microsoft WindowsXP operating system, is available for download in the Supplementary Material section on the Journal web page.

GAG length in the 3D geometric model was varied as defined by an input distribution (mean ± standard deviation). D-period bands were labeled every 67 nm along the length of the collagen fibrils and their location was not dependent on bands of neighboring fibrils. GAGs were generated by first choosing a collagen fibril and D-period band, then projecting a GAG from the band at an angle such that the GAG linked to another D-period band on a neighboring fibril. This construction is consistent with the often hypothesized aggregation of GAG chains from adjacent fibrils to create interfibrillar cross-links. GAGs were not allowed to pass through the space occupied by other GAGs or collagen fibrils (Fig. 1A).

### 2.3. Creation of 2D synthetic TEM micrographs from the 3D geometric model

A sectioning volume was created in the software to simulate the thickness of our TEM preparations (70 nm). The sectioning plane could be centered at any point into the depth of field of the model. A clipping mode allowed the user to turn off display of the collagen fibrils and GAGs outside the sectioning plane to visualize the GAG geometries within the plane (Fig. 1B). A projection feature was used to create synthetic two-dimensional TEM micro-

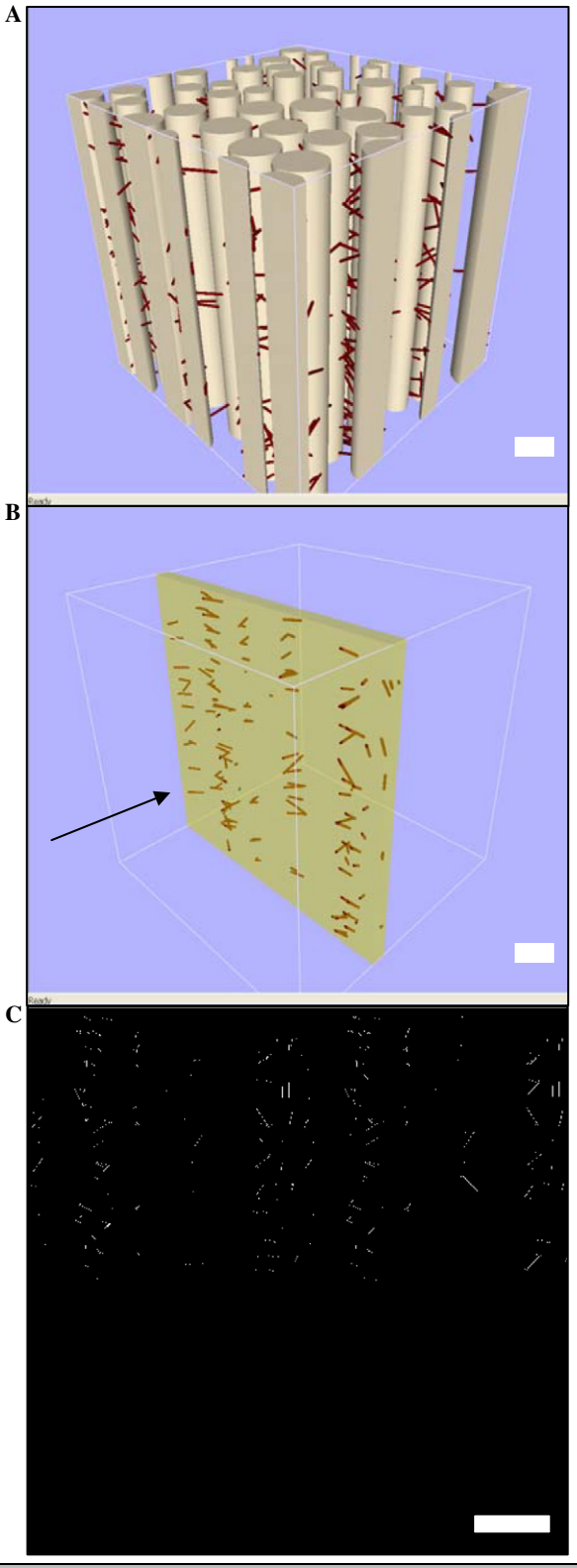


Fig. 1. Three-dimensional geometric model of a collagen and GAG matrix. (A) Example of a collagen matrix volume generated with GAGs dispersed throughout. The range of collagen fibril diameters and spacing are exaggerated to assist visualization. (B) A representative sectioning plane from the matrix in (A). GAGs within section plane are still three dimensional, but collagen and GAGs outside the section have been removed for clarity. (C) Two-dimensional projection of the three-dimensional sectioning plane. Note that discrete GAGs in three dimensions sometimes appear to overlap one another and appear shorter than their three-dimensional length. Model and sectioning plane are 1300 × 1300 nm, simulating overall dimensions of a TEM image. Arrow denotes viewing plane from which measurements were taken. Scale bars = 200 nm.

graphs by projecting the three-dimensional GAGs within the sectioning plane to the viewing plane (Fig. 1C).

Outputs from the software included GAG angle with respect to collagen fibrils and GAG length. These data were available for the entire 3D volume, within a 3D sectioning volume, and for the 2D projection planes. The synthetic two-dimensional TEM micrographs were saved for later processing. For the baseline model, 30 section planes were analyzed.

### 2.4. Model sensitivity studies

Sensitivity studies were conducted to test the relative impact of the input parameters to the 3D geometric model on the resultant GAG geometries. Seed number (nine different values), range of collagen diameter (70–90, 110–130, and 70–130 nm), GAG length (means of 50, 100, and 250 nm), and GAG concentration (three different values) were varied from the values used in the baseline model. Thus, a total of 19 different models were analyzed. Thirty sectioning volumes were captured from each of the 19 models and their GAG angle/length data and an image of each two-dimensional projection were saved to files. It is important to note that GAG concentration merely scales the model outputs. As such, all data were normalized for comparative purposes.

### 2.5. Tissue sample selection

Five human knees were obtained from five separate donors (age 47–64, median 53). Specimens remained frozen until the time of dissection. Knees were allowed to thaw and were dissected free of fat and extraneous soft tissue. Knees with surgical scars, ligament injury or cartilage degeneration characteristic of osteoarthritis were eliminated. The medial collateral ligament (MCL) was removed at both the femoral and tibial insertion sites and fine dissected to remove any overlying fascia. The ligaments were kept hydrated with normal saline throughout the tissue isolation. Bulk tissue was trimmed to remove four samples from the mid-substance of each MCL.

### 2.6. Glycosaminoglycan digestion

To isolate DS proteoglycans from other sulfated proteoglycans, enzymatic treatment with chondroitinase B (ChB) was performed on two of the four samples (randomly chosen) from each MCL, while the other two samples were used as controls. ChB specifically degrades DS (Ernst et al., 1995). All samples were equilibrated for 1 h in 15 ml of buffer (20 mM Tris, pH 7.5, 150 mM NaCl, and 5 mM $CaCl_2$) and with one tablet of Mini-Complete protease inhibitor (Roche) per 10 ml of buffer. Following the 1-h equilibration, the control samples were soaked in 15 ml of the same buffer, without protease inhibitors, for 6 h at RT. The enzymatic treatment group was soaked in 15 ml of the same buffer with 1.0 U/ml of ChB, and then soaked in a stop buffer to inhibit further ChB activity (20 mM, Tris pH 7.5, 150 mM NaCl, and 10 mM EDTA). EDTA sequesters residual calcium and inhibits ChB activity, as it is a calcium-dependent enzyme (Michel et al., 2004). All buffer treatments were performed with gentle agitation using an orbital shaker. To obtain sufficient enzyme for use in this study, ChB was cloned in *Flavobacterium heparinium* as previously described (Pojasek et al., 2001).

### 2.7. Specificity of chondroitinase B

The specificity of ChB for DS was verified by incubating stock solutions of sulfated GAGs found in ligament with ChB and then quantifying the concentration of the GAGs using an improved 1,9-dimethylmethylene blue (DMB) assay (Farndale et al., 1986). Individual reactions (30 µl, $n=6$ for each condition) were set up containing 1.0 U/ml ChB and 500 µg/ml of purified GAG (DS, chondroitin sulfate A and C, heparin sulfate, or keratin sulfate). Control reactions were set up containing GAGs and buffer only (20 mM Tris–HCl (pH 7.5), 150 mM NaCl, and 5 mM $CaCl_2$). Reactions were allowed to proceed for 6 h at RT. GAG concentrations were then quantified using the DMB assay. Five microliters of each reaction (diluted 2-fold) was transferred to a 96-well plate in duplicate, along with GAG standards. Two hundred microliters of dimethylmethylene blue reagent was added to each well, and the absorbance was immediately read in a plate reader (Synergy HT, Biotek) at 530 and 590 nm. GAG concentrations were expressed as a percentage of control reactions.

### 2.8. Chondroitinase B activity and removal of dermatan sulfate

One control and one ChB-treated sample from each knee were used to verify the removal of DS using the DMB assay. Samples were lyophilized overnight and dry weights were obtained. The samples were then incubated with 20 volumes (based on dry weight) of papain buffer for 4 h at 60 °C until the tissue was completely digested. Papain buffer consisted of 50 µg/ml papain, 50 mM sodium acetate, pH 5.5, 2 mM dithiothreitol, and 2 mM EDTA. Each extract was divided into a control and a ChB group. Twenty-five microliters of extract was mixed with 25 µl of 2× ChB buffer consisting of 0.1 U/ml ChB, 30 mM Tris, pH 8.1, 10 mM NaCl, 25 mM acetate buffer, and 5 mM $CaCl_2$. Control reactions contained the same buffer but lacked ChB. DS digestion was allowed to proceed for 2 h at RT. Total GAG content was quantified using the DMB assay in 96-well plates as described previously. The DS content of the papain extracts was calculated by subtracting the amount of GAG in the extract treated with additional ChB from that of the extract treated with additional buffer only.

### 2.9. Transmission electron microscopy

The remaining control and ChB-treated specimens from each knee were used for transmission electron microscopy



Please cite this article in press as: Henninger, H.B. et al., Spatial distribution and orientation of dermatan sulfate in human medial collateral ligament, J. Struct. Biol. (2006), doi:10.1016/j.jsb.2006.10.008

(TEM). TEM allows the visualization of sulfated GAGs by selectively targeting them with an electron-dense stain (Cribb and Scott, 1995; Haigh and Scott, 1986). Tissue was fixed in 4% paraformaldehyde with 2% glutaraldehyde overnight at 4 °C with agitation. Twenty micron sections along the sagittal plane of the ligament were obtained on a cryostat (Leica CM3050S, Exton PA) at −25 °C. Sections were mounted on slides, fixed for 30 min (2.5% glutaraldehyde, 25 mM sodium acetate, pH 5.8) and stained at critical electrolyte concentration (CEC) with 0.05% Cupromeronic Blue (CB) (2.5% glutaraldehyde, 25 mM sodium acetate, 0.1 M $MgCl_2$, and 0.05% CB, pH 5.8) for 3 h at 37 °C. At CEC, the CB selectively binds to sulfated GAGs, acting as a scaffold to support the native conformation of the molecule while reducing translocation of the molecules during further processing (Scott, 1985). Slides were contrasted for 30 min in 0.5% aqueous sodium tungstate to amplify the electron density of the CB scaffold. Specimens were then dehydrated through graded ethanol and encapsulated using Spurr's resin. Ultrathin sections (~70 nm) were obtained via ultramicrotome (Leica Ultracut UCT, Exton PA) with a diamond knife (Diatome 45°, Hatfield PA) and ribbons were floated onto 135 Hex copper grids. Grids were contrasted in aqueous uranyl acetate to visually enhance the collagen fibrils.

Digital images were collected on a Hitachi H7100 TEM with a LAB6 filament. Fields of view were selected at low magnification (1000–5000×) where intact areas of ligament were visible in the microscopic field. Edges of tissue and areas with fine sectioning artifacts were avoided. Magnification was amplified to 50 000×, the microscope was focused, and an image was collected with the integrated CCD camera. A minimum of five digital images were captured from different areas of tissue on a single grid so that an average GAG distribution could be obtained for each sample.

### 2.10. Image processing

To locate GAGs in the 2D TEM micrographs and to determine their apparent length and apparent orientation with respect to the local collagen fibrils, an image processing software pipeline was developed in Matlab using functions in the Image Processing Toolbox (Mathworks, Natick, MA). The Matlab input file is available for download as Supplementary Material on the Journal web page. The collagen fibril axis was determined by interactively digitizing four vectors along the predominant fibril axis using ImageJ (National Institutes of Health). The average angle of the collagen fibrils with respect to the horizontal was saved to a data file.

A series of morphological operations were used to eliminate background noise and reduce each detected sulfated GAG to a branched binary wireframe element, one pixel wide (Fig. 2). It should be noted that sulfated GAGs are likely aggregates of smaller GAG chains (Ernst et al., 1995; Scott, 1992). Branched GAGs are therefore either GAGs projecting off the predominant chain of the main GAG aggregate or two or more GAGs overlapping through the thickness of the specimen. As these scenarios could not be discerned using two-dimensional data, branches were broken from the main chain keeping only the longest continuous chain of pixels to represent the GAG. A size filter was applied to remove extremely small objects ($\leqslant$10 nm). These small objects were typically residual noise artifacts or GAGs exiting the viewing plane directly. In either case, such small units are subject to error in orientation processing and thus eliminated from all images.

Once wireframe elements were isolated, a principal component analysis was performed on the coordinates of the pixels of each object. This yielded a covariance matrix that was then transformed into the eigenvectors of the GAG. Taking the maximum eigenvector of each object as the definition of its orientation, the vectors associated with the GAGs were compared to the collagen fibril direction and a unique angle was quantified for each GAG with respect to the collagen fibril axis.

The synthetic 2D TEM images from the 3D geometric model were analyzed with the same image processing pipeline. Therefore, analysis of the simulation data was subject to the same overlap, branching, and length errors found in TEM images. Output data from simulation sections were the same as TEM data, including GAG lengths and orientations with respect to local collagen direction.

### 2.11. Statistical analysis

Data from the geometric models were analyzed using ANOVA with Tukey post hoc tests. Data for GAG orientation with respect to collagen fibrils and GAG length data were collapsed into discrete bins (0–10°, 11–20°, etc.) and histograms were generated. The overall number of GAGs in a simulation section and the number of GAGs at each angle and length bin were compared between and within models. Significance was set at $\alpha = 0.05$.

Results from TEM image measurements were analyzed with Kolmogorov–Smirnov (KS) tests to assess normality of data distribution. Parametric statistical analyses were preferred, but in cases with small sample sizes and/or non-normal distribution per the KS, non-parametric alternatives to the parametric tests were chosen. Significance for all tests was set at $\alpha = 0.05$. Independent *t*-tests were used to detect significant changes in the overall number of GAGs for the DMB assays as well as the image processing runs. Data for GAG orientation with respect to collagen fibrils were collapsed into discrete angle bins (0–10°, 11–20°, etc.) and histograms were generated. Independent *t*-tests were used to detect significant changes in the total number of GAGs at each individual angle bin between control and ChB-treated groups. Control and treated images for individual knees were compared using the Mann–Whitney *U* due to non-normal data distributions.



Please cite this article in press as: Henninger, H.B. et al., Spatial distribution and orientation of dermatan sulfate in human medial collateral ligament, J. Struct. Biol. (2006), doi:10.1016/j.jsb.2006.10.008

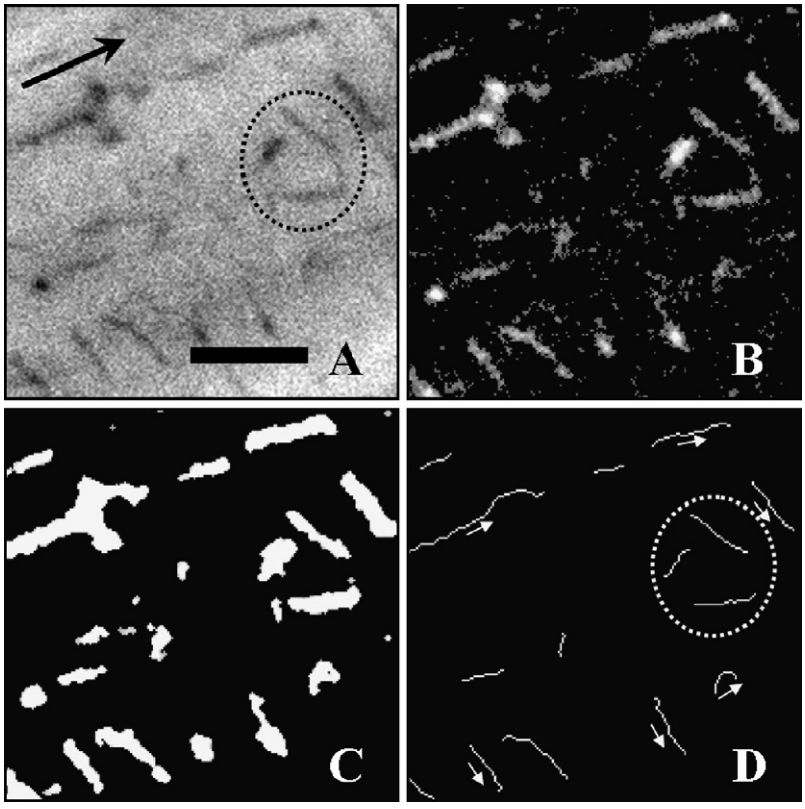


Fig. 2. Demonstration of the image processing procedure used to isolate sulfated GAGs in the TEM images and to determine their orientation angles. (A) Portion of sample image (three representative stained GAGs circled). (B) Sample image after high pass and background intensity filtering. (C) Convolved binary image improves GAG internal connectivity. (D) Wire frame representation used to calculate orientation unit vectors (arrows) of stained GAGs via principle component analysis with respect to collagen fibril axis (large arrow, (A)). As dermatan sulfate is a single polysaccharide chain, branched wire frame objects were broken and only the longest continuous chain was retained. Bar = 50 nm.

## 3. Results

### 3.1. 3D geometric model and sensitivity studies

The average collagen radius for the baseline model was $92.5 \pm 0.89$ nm, with a collagen cross-sectional area ratio of $63.3 \pm 1.6\%$. The seed number had no significant effect on GAG quantity, length, or orientation between or within models (all $p$-values $\geqslant 0.125$). Based on this finding, the results of the 10 models examining seed number were averaged to create a master baseline model.

Results for GAG angle with respect to the collagen fibril from the geometric models were plotted as a histogram (Fig. 3A). The true 3D orientation of the GAGs had very few coaxially aligned GAGs (0–10°) but increased linearly towards orthogonal orientations (81–90°). The alignment of GAGs occupying the sectioning volumes, measured with respect to the viewing plane, showed a higher percentage at coaxial orientations, but a nearly linear increasing trend towards orthogonal orientations. The orientations in 2D of GAGs projected onto the viewing plane were determined using the TEM image analysis algorithm. These GAGs were also measured with respect to the viewing plane and showed higher concentrations at coaxial orientations, but did not begin to increase in number until near orthogonal orientations (51–60°), creating a bowl-shaped distribution.

GAG length was plotted as a histogram (Fig. 3B). The true 3D orientations of the GAGs in the baseline geometric model exhibited a nearly Gaussian distribution, centered at 69 nm. This result is consistent with the input parameter to the baseline model. The apparent lengths of GAGs occupying the sectioning volumes, measured with respect to the viewing plane, were shorter due to projection. The lengths decayed steadily from a maxima at the shortest measurement of 11 nm. The lengths of GAGs projected onto the viewing plane determined using the TEM image analysis algorithm also exhibited a minima at the shortest length. The profile decayed exponentially with increasing GAG length.

Changes to collagen diameter and GAG concentration had no significant effect on the GAG length or orientation distributions (all $p$-values $\geqslant 0.125$). In contrast, changing the GAG length distribution had a dramatic effect on the GAG orientation and length profiles and magnitudes (all $p$-values $\leqslant 0.05$). Fig. 3C and D shows the angle and length predictions for two different GAG length input distributions (50, 100 nm). With respect to angle (Fig. 3C), when the prescribed GAG length input distribution was shortened, larger orthogonal populations and smaller coaxial populations of GAGs were created. Increased input GAG length had the opposite effect, increasing the entire angle distribution, especially coaxial orientations. Apparent GAG length



Please cite this article in press as: Henninger, H.B. et al., Spatial distribution and orientation of dermatan sulfate in human medial collateral ligament, J. Struct. Biol. (2006), doi:10.1016/j.jsb.2006.10.008

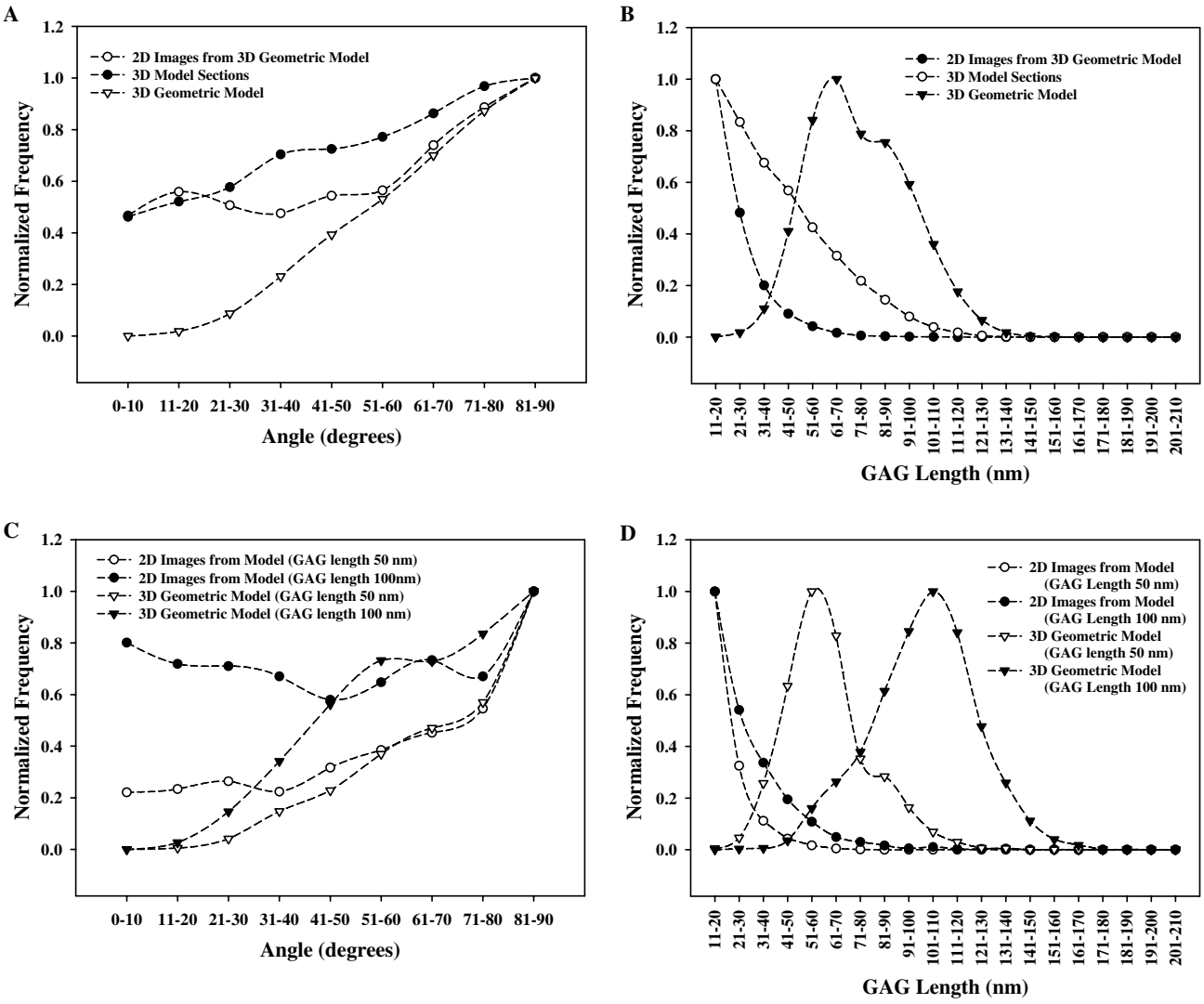


Fig. 3. GAG orientation and length from 3D model data. (A) In the 3D geometric volume, very few GAGs are coaxial, with numbers increasing towards orthogonality. GAGs contained in the section volume (3D Model sections) exhibit higher percentages of coaxial GAGs, but still trend towards orthogonality. This is due in part to interpolation error of the GAG angle as it is projected onto a plane. Two-dimensional images after image processing take on a slightly inverse Gaussian distribution, but still trends towards orthogonality. (B) GAG length distribution in the 3D model volume is centered at the input parameter ($69 \pm 23$ nm) in length. After projection of the section volume, the apparent GAG lengths are shorter. GAG lengths after image processing fall off much more steeply due to size filtering in the image processing algorithm. The difference in profile before and after processing arises from the clipping artifact when GAGs are not fully contained within the section. (C) Sensitivity of GAG orientation to changes in GAG length parameters. (D) Sensitivity of measured GAG length to changes in GAG length parameters. Increasing or decreasing the GAG length parameter causes the shape and relative magnitudes of both the 3D geometric model and 2D images to shift from baseline ((A) vs. (C), (B) vs. (D)).

showed similar trends (Fig. 3D). Decreased input GAG length shifted the normal distribution and created a steeper exponential decay in image processed data. In contrast, increased input GAG length flattened the decay resulting in an apparently longer GAG population.

### 3.2. Specificity of chondroitinase B for dermatan sulfate

ChB treatment reduced the DS standard by 77% (Fig. 4A) but had no significant effect on chondroitin sulfates A or C, heparin sulfate, or keratin sulfate ($p < 0.001$). ChB is only capable of degrading the iduronic acid containing portions of the DS stock GAG (Linhardt et al., 1991; Theocharis et al., 2001). The balance of undigested DS stock solution is likely to be the portions of the DS GAGs that contained glucuronic acid.

### 3.3. Dermatan sulfate reduction in ligament

Control specimens contained roughly $1.5 \pm 0.5$ μg of DS per milligram of tissue dry weight (Fig. 4B). Treatment with ChB significantly reduced the DS content by over 93% ($p < 0.001$). The DS content of the samples was calculated as the amount of GAG in the papain extracts that is digestible with ChB. The difference in percent reduction of DS in ligament compared to stock solution concentration of DS arises from differences in normalization.

Please cite this article in press as: Henninger, H.B. et al., Spatial distribution and orientation of dermatan sulfate in human medial collateral ligament, J. Struct. Biol. (2006), doi:10.1016/j.jsb.2006.10.008

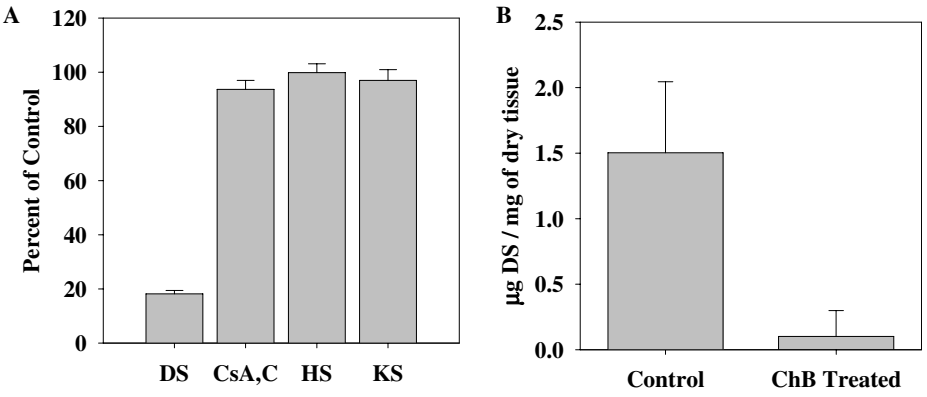


Fig. 4. Effect of chondroitinase B treatment on stock GAG solutions and treated ligament specimens. (A) Chondroitinase B (1.0 U/ml) was incubated with glycosaminoglycans (500 µg/ml) for 6 h. GAG concentration was determined using the DMB assay. Concentrations were normalized to control reactions, which did not contain ChB. DS, dermatan sulfate; CsA,C, equal mixture of chondroitin sulfates A and C; HS, heparin sulfate; KS, keratin sulfate. $N = 6$, error bars = standard deviation. (B) Reduction in dermatan sulfate concentration from control to treated ligament specimens was 93.3% ($p < 0.001$). DS content was normalized to dry weight of the specimen. $N = 5$, error bars = standard deviation.

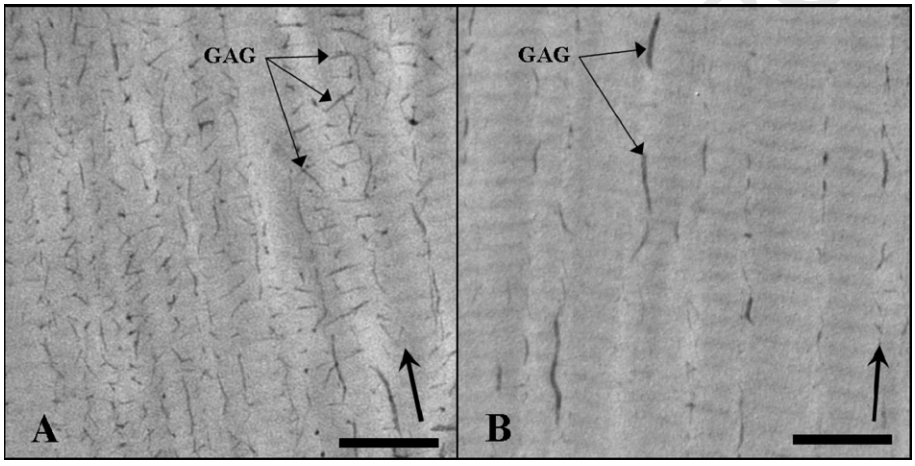


Fig. 5. Representative TEM images of medial collateral ligament stained with Cupromeronic Blue (large arrow denotes collagen fibril direction). (A) Control tissue with darkly stained sulfated GAGs. (B) Tissue treated with Chondroitinase B. Note the decrease in the number of fibril spanning sulfated GAGs and the preferred orientation of remaining GAGs along the collagen fibril direction. Bar = 200 nm.

### 3.4. Transmission electron microscopy

Images of control tissue collected via TEM exhibited typical Cupromeronic Blue staining of sulfated GAGs (Cribb and Scott, 1995; Scott, 1988; Scott and Thomlinson, 1998) (Fig. 5A). The apparent orientation of the stained GAGs was predominantly orthogonal and coaxial to the fibrils, although orientations were distributed in between these extremes as well. The apparent GAG length in control images ranged from approximately 10 nm up to 400 nm in the most extreme cases (mean $31 \pm 22$ nm). In general, the extremely long GAGs were found along collagen fibrils in the interfibrillar space between adjacent fibrils. Spacing between neighboring sulfated GAGs was observed in the expected range of the D-period band gap, roughly 60–70 nm (Pringle and Dodd, 1990; Scott, 1988; Scott and Orford, 1981). Treatment with ChB reduced the overall number of stained sulfated GAGs by 86% ($p < 0.001$) (Fig. 5B). GAGs visible after ChB digestion were generally longer than those in control images and preferentially aligned coaxial to the collagen fibrils (mean $45 \pm 13$ nm, range 10–350 nm).

### 3.5. Orientation of sulfated GAGs via image processing

The apparent angular orientation of sulfated GAGs with respect to collagen fibrils was significantly altered by ChB treatment (Fig. 6). The control tissues exhibited an inverse Gaussian distribution with relative peaks at coaxial (0–10°) and orthogonal (80–90°) orientations (median angle = 47.0°) (Fig. 6A). After ChB treatment, the apparent orientation of the remaining (non-DS) stained GAGs shifted to a positively skewed distribution (median angle = 19.7°) and showed a significant decrease in the total number of stained GAGs ($p < 0.001$).

Control and treated GAG orientation profiles were compared for each discrete angle bin. Across all knees, coaxial orientations showed a significant 69% decrease in the number of GAGs after treatment with ChB ($p < 0.001$). The percentage increased linearly with angle towards a 96%

Please cite this article in press as: Henninger, H.B. et al., Spatial distribution and orientation of dermatan sulfate in human medial collateral ligament, J. Struct. Biol. (2006), doi:10.1016/j.jsb.2006.10.008

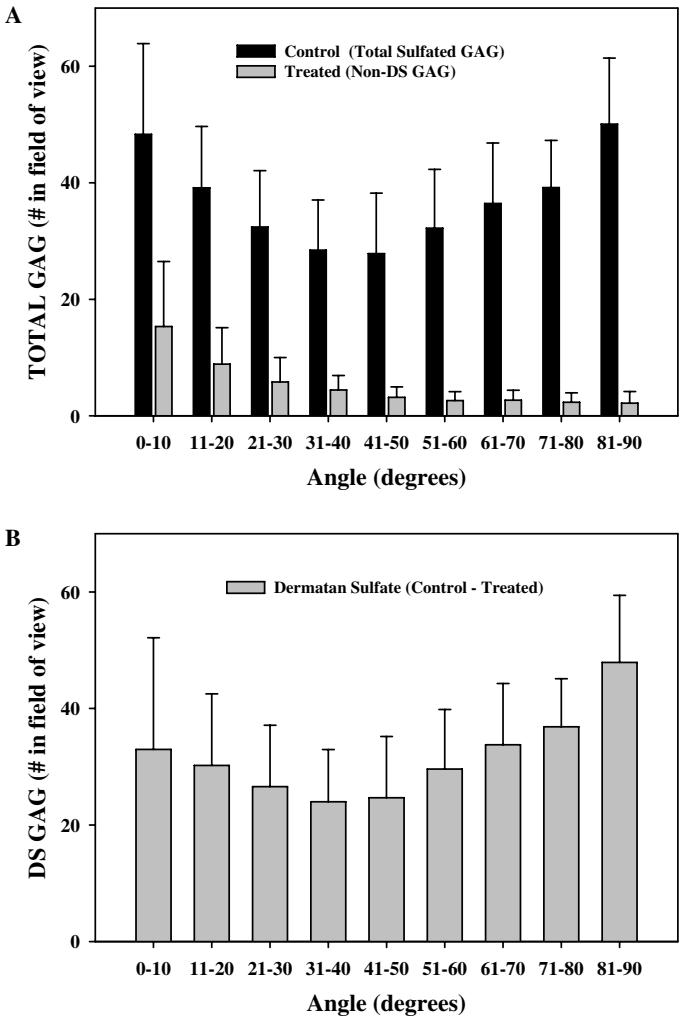


Fig. 6. Distribution of sulfated GAG angles with respect to collagen fibril orientation. (A) Sulfated GAGs in control images exhibit an inverse Gaussian distribution (median 47.0°) with relative peaks at coaxial (0–10°) and orthogonal orientations (81–90°). Non-dermatan sulfate GAGs shift to a positively skewed coaxial alignment (median 19.7°). Treatment with ChB resulted in an 86% reduction in the number of sulfated GAGs ($p < 0.001$). GAGs were significantly reduced by a minimum of 69% (coaxial) up to roughly 95% at orthogonal orientations ($p < 0.001$). (B) Distribution of dermatan sulfate angle with respect to collagen fibril orientation. Dermatan sulfate exhibited an inverse Gaussian distribution (median 55°) trending from a minor peak at coaxial orientation to a predominant peak at orthogonal orientation. $N = 5$, error bars = standard deviation.

reduction at orthogonal orientations. Analysis of the GAG reduction by angle bin in individual knees showed a similar trend. Of the five knees examined, four knees exhibited a significant decrease in all angle bins ($p < 0.001$). The final knee showed significant decreases in the number of GAGs in all angle bins except one, the coaxial orientation ($p < 0.001$ and $p = 0.81$, respectively).

The apparent orientation of DS with respect to collagen fibrils was derived by subtracting the treated distribution profile from the control distribution profile (Fig. 6B). DS alone exhibited a less dramatic inverse Gaussian distribution than control samples. DS distribution was negatively skewed (median angle = 55.0°) with a minor peak at coaxial alignment and a predominant peak at orthogonal orientations. From this profile it was estimated that nearly 60% of DS GAGs are oriented at angles greater than 45° with respect to collagen fibrils.

## 4. Discussion

Interpretation of the results from the analysis of the 3D baseline geometric model provides an understanding of the errors in measurement of apparent length and orientation from 2D TEM micrographs due to projection. The stained GAGs in 2D TEM micrographs may be oriented so that they leave the plane of section. Measurement of the 2D in-plane GAG length underestimates the true length by some factor of the cosine of the through-thickness angle with respect to the plane. Also, TEM sections are simply slices through native tissue without regard to the position of the structure in the depth of field. Without *a priori* knowledge of the underlying geometric structure, one cannot presume to know which stained GAGs were cleaved in the sectioning process and which were contained wholly within the preparation. Modeling the collagen/GAG geometry in 3D pro-

Please cite this article in press as: Henninger, H.B. et al., Spatial distribution and orientation of dermatan sulfate in human medial collateral ligament, J. Struct. Biol. (2006), doi:10.1016/j.jsb.2006.10.008

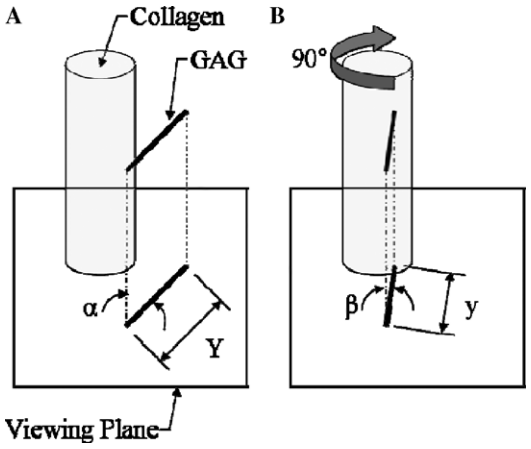


Fig. 7. Schematic of errors in measurement of apparent orientation and length due to projection onto a viewing plane. (A) Collagen fibril with a GAG parallel to the viewing plane. When projected, the GAG length and orientation in the 2D plane will reflect the true length ($Y$) and true angle ($\alpha$) with respect to the fibril. (B) Rotate the same collagen fibril and GAG 90° so the GAG is extended into the viewing plane. The GAG has the same length and angle in three dimensions, but the projected length and orientation are shorter ($y$) and more coaxial ($\beta$) with respect to the fibril.

vides the necessary *a priori* information to interpret the 2D TEM image data. As shown in Fig. 3, the distributions of apparent GAG angle and length change when the image data are projected to two dimensions. The apparent number of GAGs aligned at coaxial orientations increases dramatically after 2D projection, both in simple projection and after image processing of the planar projection (Fig. 3A). Since the true orientation of the GAG population was much more orthogonal than coaxial as shown by the volume data (Fig. 3A, filled triangles), this is an artifact. Within the entire volume, GAG angle was measured with respect to the collagen fibril from which it originated. A GAG extending from a fibril parallel to the viewing plane would retain the true angle since projection simply maps it onto the viewing plane (Fig. 7A). In contrast, a GAG extending from a fibril toward the viewing plane would appear more vertical with the respect to the viewing plane (Fig. 7B). Therefore, the projection error is primarily due to the orientation of GAGs relative to the viewing plane rather than their orientation with respect to the collagen fibril.

When the lengths of GAGs in the 3D geometric model were analyzed, the GAG length distribution was as described by the input parameter in a nearly Gaussian profile (Fig. 3B, filled triangles). Projection onto a 2D plane significantly shortened the apparent GAG lengths until their maxima were at the shortest measurable length (Fig. 3B, open circles). Further image processing of the projected planar image intensified this effect, creating a maxima at the shortest length and an exponential decay in frequency with increasing length (Fig. 3B, filled circles). In order to reduce noise artifacts in measures of angle and GAG length in TEM images, a size filter is applied to remove any GAGs below 10 nm since they are more prone to misinterpretation against background noise.

Pertaining to MCL specimens, the biochemical analyses demonstrated that ChB treatment was effective in eliminating DS GAGs, allowing us to examine their orientation as a subpopulation when compared to all sulfated GAGs. Up to 96% of DS in human MCL specimens was removed by enzymatic digestion, while TEM image processing resulted in a total sulfated GAG reduction on the order of 86% (in terms of number, not weight). This demonstrates that DS is the predominant sulfated GAG in the human MCL. Previous studies have reported that, purely by number, the majority of PGs in connective tissue are decorin with its associated DS side chain (Amiel et al., 1990; Raspanti et al., 1997; Scott, 1988; Vogel et al., 1993). Studies in bovine ligament and human tendon have shown that while decorin/DS comprise up to 90% of the PGs in ligament by number, smaller concentrations of biglycan and versican are present (Campbell et al., 1996; Ilic et al., 2005; Vogel et al., 1993). These proteoglycans may both contain GAG chains of chondroitin sulfates A and C, the likely sulfated GAGs present in ligament after ChB treatment. Traces of aggrecan, a PG that contains numerous keratin sulfate and chondroitin sulfate side chains, may also be found in extremely small concentrations but are much more prevalent in other musculoskeletal soft tissues such as articular cartilage.

The apparent orientation and length data obtained from analysis of the 2D TEM sections can be interpreted in the context of the 3D geometric model to determine the appropriateness of the assumptions of the 3D geometric model and to interpret the results of the 2D TEM measurements. Analysis of the 2D TEM images showed that DS GAGs were apparently oriented at all angles with respect to the collagen fibrils (Fig. 6A and B). However, these data are subject to the projection errors discussed previously. Fig. 8 shows the GAG angle distribution from the 2D TEM images from Fig. 6B and the GAG length distribution from the 2D TEM images (not shown previously), plotted with the results from the 3D geometric model from Fig. 3. Simulation data from Fig. 3 were generated using a population with a GAG length describing only DS, not the longer non-DS GAG chains. The GAG apparent length and angle data from the 2D TEM images are in very good agreement with the projected and processed data from the 3D model in both angle (Fig. 8A) and length (Fig. 8B). In both cases, the distributions from the 2D TEM images are nearly identical to the distributions from the baseline 3D geometric model. This strongly suggests that the length distribution used in the baseline model ($69 \pm 23$ nm, (Morgelin et al., 1989)) provides a realistic description of DS length distribution in human MCL. Furthermore, it is clear from Fig. 3C and D that the angle and length distributions from the 3D model are highly sensitive to the assumed GAG length distribution, further supporting the interpretation of our experimental TEM data with the results of the baseline 3D geometric model.

Analysis of the GAG orientations with respect to the collagen fibrils demonstrated distinct differences between DS and non-DS species within human ligament. Non-DS



Please cite this article in press as: Henninger, H.B. et al., Spatial distribution and orientation of dermatan sulfate in human medial collateral ligament, J. Struct. Biol. (2006), doi:10.1016/j.jsb.2006.10.008

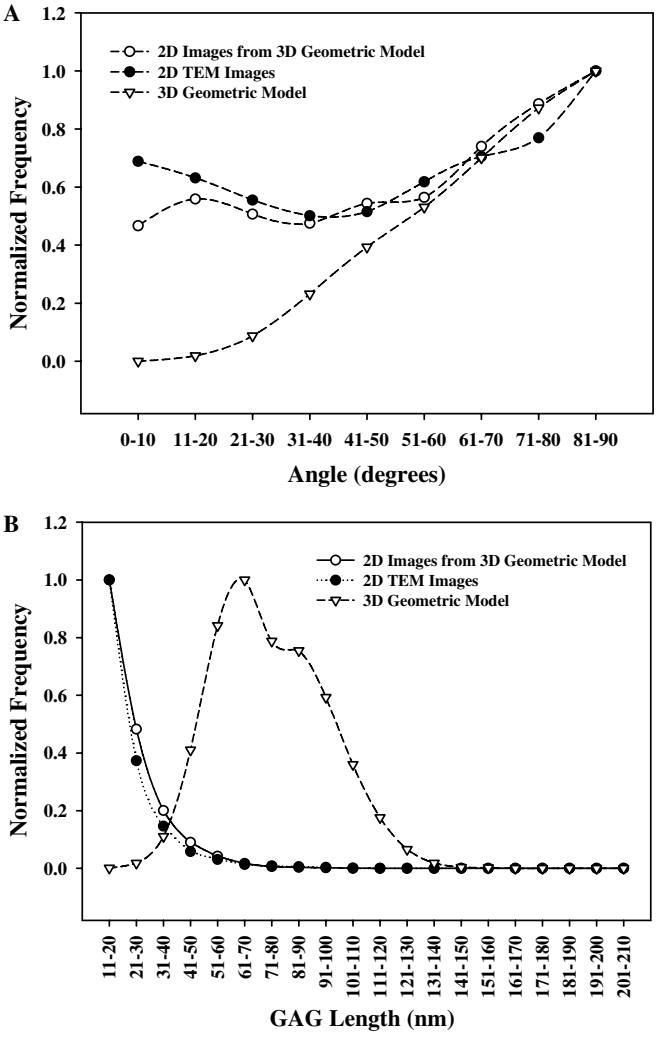


Fig. 8. Data from the 3D geometric model and 2D TEM images for GAG angle and length. (A) Histograms of GAG angle with respect to collagen fibril. Measurements from the 2D synthetic images generated from the 3D geometric model (open circles) are in very good agreement with the 2D TEM data (closed circles). (B) Histograms of GAG length. Again the measurements from the 2D synthetic images generated using the 3D geometric model are in excellent agreement with measurements from the 2D TEM images, with a peak at the smallest length and exponential decay as length increases. The agreement between the measurements from the 2D synthetic images and the 2D TEM images demonstrates that the baseline model accurately describes GAG length and distribution in the collagen matrix. Thus, the true underlying distributions are similar to the predictions from the baseline 3D geometric model (open triangles).

GAGs preferred coaxial alignment with collagen fibrils and were longer than DS GAGs, whereas DS GAGs trended towards orthogonality but were found in all orientations with some regularity. In a study by Morgelin et al. (1989), average decorin GAG chain length was 69 nm, while a group of large PGs, when extended, had core protein lengths up to 300 nm. The results of a study of bovine tendon and ligament using TEM agree with the sulfated GAG length ranges stated previously, as well as the observation that smaller GAGs spanned fibrils while larger GAGs were typically found between and along collagen fibrils (Van Kuppevelt et al., 1987). The molecular weight range of the larger GAGs in their study was 165–200 kDa, consistent with previous observations of aggrecan.

Until this study, most observations of the distribution of DS focused on GAG species determination and the binding site between decorin and collagen fibrils (Cribb and Scott, 1995; Kuwaba et al., 2001; Scott and Orford, 1981; Scott and Thomlinson, 1998; Van Kuppevelt et al., 1987). These studies qualitatively described the sulfated GAGs as orthogonal to the collagen fibrils, but did not necessarily distinguish between the subpopulations of sulfated GAGs and their specific orientations. Although our results demonstrate that DS does indeed prefer orthogonal orientations, almost 40% of DS GAGs were oriented across a range of angles around and along the collagen fibril, a significant proportion of the overall DS population that had previously been overlooked. This is in agreement with qualitative observations from atomic force and scanning electron microscopy of the rat tail tendon (Raspanti et al., 1997, 2002), which demonstrated that a network of thin filaments wrap along the surface or span between neighboring collagen fibrils. In these studies, treatment with chondroitinase ABC removed these thin filaments, suggesting that the GAGs were DS and/or chondroitin sulfates A and C.

The observed size and orientation of the sulfated GAGs may be indicative of their potential functional roles. Large proteoglycans such as versican and aggrecan are associated with large numbers of peripheral GAGs like chondroitin sulfates A and C and keratin sulfate. The large number of localized GAGs and their high electronegativity allows them to trap large amounts of water. They are found in large quantities in highly hydrated tissues like articular cartilage that experience primarily hydrostatic loading conditions (Basalo et al., 2004; Frank et al., 1987; Seog et al., 2005; Theocharis et al., 2001; Zhu et al., 1993). The presence of versican and aggrecan in ligament may suggest similar physiological roles. As they appear to be found between collagen fibrils and orientated coaxially, the presence of a highly hydrated PG would provide resistance to water movement through the tissue while possibly acting as a lubricant as adjacent collagen fibrils slide relative to one another.

In contrast, DS GAGs were much smaller than the large non-DS GAGs in the TEM images and they were preferentially orientated in a fibril spanning position, although they could be found at all angles with respect to collagen. There were significantly more DS molecules than non-DS molecules. Decorin/DS has been implicated in limiting collagen fibril diameter and controlling fibril spacing (Iozzo, 1998), and it has been suggested that the DS GAGs may link adjacent fibrils and transmit mechanical forces in various fibrous tissues (Danielson et al., 1997; Liu et al., 2005; Pins et al., 1997; Redaelli et al., 2003; Robinson et al., 2005; Scott, 2003; Scott and Thomlinson, 1998; Vesentini et al., 2005). DS may act as a spacer between fibrils by surrounding the collagen fibril bundles, ensuring repeatable spacing, while self-associating with other DS molecules from neighboring fibrils to keep the network intact.

Please cite this article in press as: Henninger, H.B. et al., Spatial distribution and orientation of dermatan sulfate in human medial collateral ligament, J. Struct. Biol. (2006), doi:10.1016/j.jsb.2006.10.008

A potential limitation, artifacts arising from the image processing pipeline may influence the distribution of GAGs, as the algorithms are not without bias. The "art" of image processing has no gold standard, since even raw images must first be interpreted by a human to determine what data in the field of view are valid. That said, algorithms to remove background noise and to detect stained GAGs can only be evaluated by simple comparison of raw images with processed images. From there it is the observation and interpretation of the viewer that determines what is an acceptable result. In this study, a small population of raw images was manually compared to their line element counterparts. Features under scrutiny were the shape, orientation, and position of GAGs with respect to their neighbors. It was found that all stated characteristics of detected GAGs agreed very well against raw images, but up to 5% of GAGs were either not detected or were detected erroneously. These errors would be expected to be found in any set of images, and as this was a comparative study, the difference between control and treated cases would essentially result in error cancellation.

In conclusion, a 3D geometric model of collagen fibrils and GAGs was constructed, analyzed, and then used to interpret the results of measurements of sulfated GAGs in human medial collateral ligament from TEM micrographs. An image processing pipeline was developed and used to segment sulfated GAGs in digital TEM images, to determine their orientation with respect to their local collagen fibrils, and to quantify their apparent length. The 3D model allowed accurate interpretation of geometric measurements from 2D TEM images by interpolating the differences between volumetric orientation and geometries and their respective projections into two dimensions. DS was the predominant sulfated GAG in the mid-substance of human MCL by number, and it was most often found in orientations spanning adjacent fibrils. A significant proportion of DS GAGs, up to 40%, were found at angles not associated with fibril spanning orientations. Non-DS sulfated GAGs, however, were oriented almost exclusively along the long axis of the collagen fibrils. These data provide a foundation for improvements of models simulating the fibril linking capabilities of DS GAGs, which to date have only assumed a simplified orthogonal GAG arrangement. However, only direct mechanical experimentation of the microenvironment of connective tissues will be able to conclusively determine if DS provides structural support in connective tissues.

## Acknowledgment

Financial support from NIH #AR47369 is gratefully acknowledged.

## References

Amiel, D., Billings, E., Akeson, W., 1990. Ligament structure, chemistry, and physiology. In: Daniel, D. (Ed.), Knee Ligaments Structure, Function, Injury, and Repair. Raven Press, New York, pp. 71–91.

Amiel, D., Frank, C., Harwood, F., Fronek, J., Akeson, W., 1984. Tendons and ligaments: a morphological and biochemical comparison. J. Orthop. Res. 1, 257–265.

Baek, G.J., Carlin, G.H., Vogrin, T.M., Woo, S.L., Harner, C.D., 1998. Quantitative analysis of collagen fibrils of human cruciate and meniscofemoral ligaments. Clin. Orthop. Relat. Res., 205–211.

Basalo, I.M., Mauck, R.L., Kelly, T.A., Nicoll, S.B., Chen, F.H., Hung, C.T., Ateshian, G.A., 2004. Cartilage interstitial fluid load support in unconfined compression following enzymatic digestion. J. Biomech. Eng. 126, 779–786.

Campbell, M.A., Tester, A.M., Handley, C.J., Checkley, G.J., Chow, G.L., Cant, A.E., Winter, A.D., Cain, W.E., 1996. Characterization of a large chondroitin sulfate proteoglycan present in bovine collateral ligament. Arch. Biochem. Biophys. 329, 181–190.

Chopra, C.H., Pearson, R.K., Pringle, G.A., Fackre, D.S., Scott, P.G., 1985. Dermatan sulphate is located on serine-4 of bovine skin proteodermatan sulphate. Demonstration that most molecules possess only one glycosaminoglycan chain and comparison of amino acid sequences around glycosylation sites in different proteoglycans. Biochem. J. 232, 277–279.

Cribb, A.M., Scott, J.E., 1995. Tendon response to tensile stress: an ultrastructural investigation of collagen:proteoglycan interactions in stressed tendon. J. Anat. 187 (Pt. 2), 423–428.

Danielson, K.G., Baribault, H., Holmes, D.F., Graham, H., Kadler, K.E., Iozzo, R.V., 1997. Targeted disruption of decorin leads to abnormal collagen fibril morphology and skin fragility. J. Cell Biol. 136, 729–743.

Ernst, S., Langer, R., Cooney, C.L., Sasisekharan, R., 1995. Enzymatic degradation of glycosaminoglycans. Crit. Rev. Biochem. Mol. Biol. 30, 387–444.

Farndale, R.W., Buttle, D.J., Barrett, A.J., 1986. Improved quantitation and discrimination of sulphated glycosaminoglycans by use of dimethylmethylene blue. Biochim. Biophys. Acta 883, 173–177.

Frank, C., Bray, D., Rademaker, A., Chrusch, C., Sabiston, P., Bodie, D., Rangayyan, R., 1989. Electron microscopic quantification of collagen fibril diameters in the rabbit medial collateral ligament: a baseline for comparison. Connect. Tissue Res. 19, 11–25.

Frank, E.H., Grodzinsky, A.J., Koob, T.J., Eyre, D.R., 1987. Streaming potentials: a sensitive index of enzymatic degradation in articular cartilage. J. Orthop. Res. 5, 497–508.

Fung, D.T., Ng, M.C., Leung, G.Y., Tay, D.K., 2003. Investigation of the collagen fibril distribution in the medial collateral ligament in a rat knee model. Connect. Tissue Res. 44, 2–11.

Gillard, G.C., Merrilees, M.J., Bell-Booth, P.G., Reilly, H.C., Flint, M.H., 1977. The proteoglycan content and the axial periodicity of collagen in tendon. Biochem. J. 163, 145–151.

Goldoni, S., Owens, R.T., McQuillan, D.J., Shriver, Z., Sasisekharan, R., Birk, D.E., Campbell, S., Iozzo, R.V., 2004. Biologically active decorin is a monomer in solution. J. Biol. Chem. 279, 6606–6612.

Haigh, M., Scott, J.E., 1986. A method of processing tissue sections for staining with cu-promeronic blue and other dyes, using CEC techniques, for light and electron microscopy. Basic. Appl. Histochem. 30, 479–486.

Hart, R.A., Akeson, W.H., Spratt, K., Amiel, D., 1999. Collagen fibril diameter distributions in rabbit anterior cruciate and medial collateral ligaments: changes with maturation. Iowa Orthop. J. 19, 66–70.

Ilic, M.Z., Carter, P., Tyndall, A., Dudhia, J., Handley, C.J., 2005. Proteoglycans and catabolic products of proteoglycans present in ligament. Biochem. J. 385, 381–388.

Iozzo, R.V., 1998. Matrix proteoglycans: from molecular design to cellular function. Annu. Rev. Biochem. 67, 609–652.

Kuwaba, K., Kobayashi, M., Nomura, Y., Irie, S., Koyama, Y., 2001. Elongated dermatan sulphate in post-inflammatory healing skin distributes among collagen fibrils separated by enlarged interfibrillar gaps. Biochem. J. 358, 157–163.

Linhardt, R.J., al-Hakim, A., Liu, J.A., Hoppensteadt, D., Mascellani, G., Bianchini, P., Fareed, J., 1991. Structural features of dermatan sulfates and their relationship to anticoagulant and antithrombotic activities. Biochem. Pharmacol. 42, 1609–1619.

Liu, X., Yeh, M.L., Lewis, J.L., Luo, Z.P., 2005. Direct measurement of the rupture force of single pair of decorin interactions. Biochem. Biophys. Res. Commun. 338, 1342–1345.

Lo, I.K., Marchuk, L.L., Leatherbarrow, K.E., Frank, C.B., Hart, D.A., 2004. Collagen fibrillogenesis and mRNA levels in the maturing rabbit medial collateral ligament and patellar tendon. Connect. Tissue Res. 45, 11–22.

Michel, G., Pojasek, K., Li, Y., Sulea, T., Linhardt, R.J., Raman, R., Prabhakar, V., Sasisekharan, R., Cygler, M., 2004. The structure of chondroitin B lyase complexed with glycosaminoglycan oligosaccharides unravels a calcium-dependent catalytic machinery. J. Biol. Chem. 279, 32882–32896.

Morgelin, M., Paulsson, M., Malmstrom, A., Heinegard, D., 1989. Shared and distinct structural features of interstitial proteoglycans from different bovine tissues revealed by electron microscopy. J. Biol. Chem. 264, 12080–12090.

Pins, G.D., Christiansen, D.L., Patel, R., Silver, F.H., 1997. Self-assembly of collagen fibers. Influence of fibrillar alignment and decorin on mechanical properties. Biophys. J. 73, 2164–2172.

Pojasek, K., Shriver, Z., Kiley, P., Venkataraman, G., Sasisekharan, R., 2001. Recombinant expression, purification, and kinetic characterization of chondroitinase AC and chondroitinase B from *Flavobacterium heparinium*. Biochem. Biophys. Res. Commun. 286, 343–351.

Pringle, G.A., Dodd, C.M., 1990. Immunoelectron microscopic localization of the core protein of decorin near the d and e bands of tendon collagen fibrils by use of monoclonal antibodies. J. Histochem. Cytochem. 38, 1405–1411.

Raspanti, M., Congiu, T., Guizzardi, S., 2002. Structural aspects of the extracellular matrix of the tendon: an atomic force and scanning electron microscopy study. Arch. Histol. Cytol. 65, 37–43.

Raspanti, M., Alessandrini, A., Ottani, V., Ruggeri, A., 1997. Direct visualization of collagen-bound proteoglycans by tapping-mode atomic force microscopy. J. Struct. Biol. 119, 118–122.

Redaelli, A., Vesentini, S., Soncini, M., Vena, P., Mantero, S., Montevecchi, F.M., 2003. Possible role of decorin glycosaminoglycans in fibril to fibril force transfer in relative mature tendons—a computational study from molecular to microstructural level. J. Biomech. 36, 1555–1569.

Robinson, P.S., Huang, T.F., Kazam, E., Iozzo, R.V., Birk, D.E., Soslowsky, L.J., 2005. Influence of decorin and biglycan on mechanical properties of multiple tendons in knockout mice. J. Biomech. Eng. 127, 181–185.

Scott, J.E., 1985. Proteoglycan histochemistry—a valuable tool for connective tissue biochemists. Coll. Relat. Res. 5, 541–575.

Scott, J.E., 1988. Proteoglycan–fibrillar collagen interactions. Biochem. J. 252, 313–323.

Scott, J.E., 1992. Supramolecular organization of extracellular matrix glycosaminoglycans, in vitro and in the tissues. FASEB J. 6, 2639–2645.

Scott, J.E., 1996. Proteodermatan and proteokeratan sulfate (decorin, lumican/fibromodulin) proteins are horseshoe shaped Implications for their interactions with collagen. Biochemistry 35, 8795–8799.

Scott, J.E., 2001. Structure and function in extracellular matrices depend on interactions between anionic glycosaminoglycans. Pathol. Biol. (Paris) 49, 284–289.

Scott, J.E., 2003. Elasticity in extracellular matrix 'shape modules' of tendon, cartilage, etc. A sliding proteoglycan-filament model. J. Physiol. 553, 335–343.

Scott, J.E., Orford, C.R., 1981. Dermatan sulphate-rich proteoglycan associates with rat tail-tendon collagen at the d band in the gap region. Biochem. J. 197, 213–216.

Scott, J.E., Thomlinson, A.M., 1998. The structure of interfibrillar proteoglycan bridges (shape modules') in extracellular matrix of fibrous connective tissues and their stability in various chemical environments. J. Anat. 192 (Pt. 3), 391–405.

Scott, P.G., McEwan, P.A., Dodd, C.M., Bergmann, E.M., Bishop, P.N., Bella, J., 2004. Crystal structure of the dimeric protein core of decorin, the archetypal small leucine-rich repeat proteoglycan. Proc. Natl. Acad. Sci. USA 101, 15633–15638.

Seog, J., Dean, D., Rolauffs, B., Wu, T., Genzer, J., Plaas, A.H., Grodzinsky, A.J., Ortiz, C., 2005. Nanomechanics of opposing glycosaminoglycan macromolecules. J. Biomech. 38, 1789–1797.

Silver, F.H., Freeman, J.W., Seehra, G.P., 2003. Collagen self-assembly and the development of tendon mechanical properties. J. Biomech. 36, 1529–1553.

Theocharis, D.A., Papageorgacopoulou, N., Vynios, D.H., Anagnostides, S.T., Tsiganos, C.P., 2001. Determination and structural characterisation of dermatan sulfate in the presence of other galactosaminoglycans. J. Chromatogr. B Biomed. Sci. Appl. 754, 297–309.

Trowbridge, J.M., Gallo, R.L., 2002. Dermatan sulfate: new functions from an old glycosaminoglycan. Glycobiology 12, 117R–125R.

Van Kuppevelt, T.H., Rutten, T.L., Kuyper, C.M., 1987. Ultrastructural localization of proteoglycans in tissue using cuprolinic blue according to the critical electrolyte concentration method: comparison with biochemical data from the literature. Histochem. J. 19, 520–526.

Venkataraman, G., Sasisekharan, V., Cooney, C.L., Langer, R., Sasisekharan, R., 1994. A stereochemical approach to pyranose ring flexibility: its implications for the conformation of dermatan sulfate. Proc. Natl. Acad. Sci. USA 91, 6171–6175.

Vesentini, S., Redaelli, A., Montevecchi, F.M., 2005. Estimation of the binding force of the collagen molecule-decorin core protein complex in collagen fibril. J. Biomech. 38, 433–443.

Vogel, K.G., Paulsson, M., Heinegard, D., 1984. Specific inhibition of type I and type II collagen fibrillogenesis by the small proteoglycan of tendon. Biochem. J. 223, 587–597.

Vogel, K.G., Ordog, A., Pogany, G., Olah, J., 1993. Proteoglycans in the compressed region of human tibialis posterior tendon and in ligaments. J. Orthop. Res. 11, 68–77.

Weber, I.T., Harrison, R.W., Iozzo, R.V., 1996. Model structure of decorin and implications for collagen fibrillogenesis. J. Biol. Chem. 271, 31767–31770.

Zhu, W., Mow, V.C., Koob, T.J., Eyre, D.R., 1993. Viscoelastic shear properties of articular cartilage and the effects of glycosidase treatments. J. Orthop. Res. 11, 771–781.



Please cite this article in press as: Henninger, H.B. et al., Spatial distribution and orientation of dermatan sulfate in human medial collateral ligament, J. Struct. Biol. (2006), doi:10.1016/j.jsb.2006.10.008